Numerical Solution of the Coupled-Power Equation in Step-Index Optical Fibers

MICHEL ROUSSEAU AND LUC JEUNHOMME

Abstract—**By use of the finite-difference method of numerical analysis, a simple numerical solution is obtained for the coupled-power equation in optical fibers. For a specified arbitrary coupling coefficient and launching condition, the solution yields all the quantities of interest in the interior of the fiber: power distribution, attenuation, and far-field radiation pattern as functions of length. Results for buffered and cabled Corning fibers are reported. Attention is mainly focused on the influence of the microbends on the optical losses.**

I. Introduction

In using a multimode optical fiber as a transmission link, one is concerned about the propagation characteristics under practical conditions. The manufacturing, buffering, and cabling of the fiber introduce irregularities in the index distribution and the waveguide geometry. These deviations from the perfect straight waveguide produce a coupling of the power of one guided mode to the others, and therefore induce excess losses.

In an attempt to explain the mode coupling process and to allow quantitative predictions, Gloge has developed a power flow equation [1]. In order to derive analytical solutions, it is assumed that the differential attenuation $\alpha(\theta)$ (attenuation of a mode of angle θ minus the attenuation of mode with $\theta = 0$) has parabolic variation and the coupling coefficient $C(\theta)$ is constant [1], [2]. These assumptions lead to far-field radiation patterns that theoretically extend to infinity and to pulse broadening greater than those experimentally obtained.

As a second approach in mode coupling understanding, we have to take experimental results into account. It has been observed [3], [4] that the attenuation $\alpha(\theta)$ is nearly constant but becomes infinite for angle θ greater than the maximum guiding angle θ_M, and that the coupling coefficient $C(\theta)$ is not always constant. However, the corresponding equation cannot be treated analytically for different launching conditions.

It is the purpose of this paper to present a numerical method of solution of the more realistic coupled power equation. The power density is sought throughout the whole length of the fiber for arbitrary coupling coefficients and launching conditions.

After a short derivation of the basic equation (Section II), the formal treatment and the difference schemes used are given in Section III. The physical significance of the results is discussed in Section IV.

Manuscript received June 14, 1976; revised December 20, 1976.
The authors are with the Laboratoires de Marcoussis, Centre de Recherche, Compagnie Générale d'Électricité, Marcoussis, France.

II. Basic Equation

By assuming that the difference in refractive index of core n_1 and cladding n_2 is very slight, Gloge [1] has shown that the discrete mode spectrum can be approximated by a modal continuum. The continuous variable is the propagation angle θ to the fiber axis related to the propagation constant β of the corresponding mode by

$$\beta = \frac{2\pi n_1}{\lambda} \cos\theta \tag{1}$$

where λ is the free-space wavelength.

The maximum angle θ_M is given by the condition for total internal reflection

$$\theta_M = \arccos\frac{n_2}{n_1} \simeq \sqrt{2\left(1 - \frac{n_2}{n_1}\right)}. \tag{2}$$

We deduce the numerical aperture

$$NA = n_1 \sin\theta_M \simeq \sqrt{2n_1(n_1 - n_2)}. \tag{3}$$

The angular separation between adjacent modes is constant and given by

$$\delta\theta = \frac{\lambda}{4an_1} \tag{4}$$

where a is the core radius.

With the additional assumption of mode coupling only between adjacent modes, Gloge obtained the fundamental coupled-power equation

$$\frac{\partial P(\theta,z)}{\partial z} = -\alpha(\theta)P(\theta,z) + \frac{\delta\theta^2}{\theta}\frac{\partial}{\partial\theta}\left[\theta C(\theta)\frac{\partial P(\theta,z)}{\partial\theta}\right] \tag{5}$$

where

- $P(\theta,z)$ power distribution per unit solid angle at a point z;
- $C(\theta)$ coupling coefficient;
- $\alpha(\theta)$ modal attenuation.

As has been experimentally observed [3], [4], the attenuation remains constant throughout the guided modes region and rises very rapidly in the radiation-modes region. Thus

$$\begin{aligned} \alpha(\theta) &= \alpha_0, \qquad 0 \le \theta \le \theta_M \\ \alpha(\theta) &= \infty, \qquad \theta_M < \theta. \end{aligned} \tag{6}$$

By substituting (6) into (5), we obtain a loss term $-\alpha_0 P(\theta,z)$. This leads to a multiplying factor $\exp(-\alpha_0 z)$ in the solution that represents conventional losses (absorption and scattering). In the work that follows we neglect this component

and only consider the coupling-induced losses. With this simplification (5) is reduced to

$$\frac{\partial P(\theta,z)}{\partial z} = \frac{\delta\theta^2}{\theta}\frac{\partial}{\partial\theta}\left[\theta C(\theta)\frac{\partial P(\theta,z)}{\partial\theta}\right], \qquad 0 \le \theta \le \theta_M$$
$$P(\theta,z) = 0, \qquad \theta_M < \theta. \tag{7}$$

It is convenient to introduce a normalized coupling coefficient

$$D(\theta) = C(\theta)\delta\theta^2. \tag{8}$$

Hence (7) in the guided modes region becomes

$$\theta\frac{\partial P}{\partial z} = \frac{\partial}{\partial\theta}\left[\theta D(\theta)\frac{\partial P}{\partial\theta}\right]. \tag{9}$$

The boundary conditions are

$$P(\theta_M,z) = 0$$
$$D(\theta)\left.\frac{\partial P}{\partial\theta}\right|_{\theta=0} = 0. \tag{10}$$

The last condition indicates that coupling is limited to propagation modes (i.e., $\theta > 0$). The total power at length z is

$$\mathcal{P}(z) = 2\pi\int_0^{\theta_M} \sin\theta P(\theta,z)\,d\theta$$

under the assumption of weakly guiding fibers

$$\mathcal{P}(z) = 2\pi\int_0^{\theta_M} \theta P(\theta,z)\,d\theta. \tag{11}$$

Using (9), this gives

$$\frac{d\mathcal{P}(z)}{dz} = 2\pi\theta_M D(\theta_M)\left.\frac{\partial P}{\partial\theta}\right|_{\theta=\theta_M} \tag{12}$$

This relationship will be used to test the consistency of the numerical method and to estimate the achieved accuracy (Section III).

Let us briefly examine the case where the coupling coefficient is constant. With

$$D(\theta) = D_0 \tag{13}$$

(9) may be written

$$\frac{\partial P}{\partial Z} = \frac{1}{\theta}\frac{\partial}{\partial\theta}\left[\theta\frac{\partial P}{\partial\theta}\right] \tag{14}$$

where Z is the normalized length

$$Z = D_0 z. \tag{15}$$

The integration of (14) may be performed by separation of the variables. The result is [6]

$$P(\theta,Z) = \sum_{i=0}^{\infty}\eta_i \exp(-\Gamma_i Z)J_0(\sqrt{\Gamma_i}\,\theta). \tag{16}$$

The expansion coefficient η_i depends on the launching condition at $z = 0$, and the loss coefficient Γ_i is related to the ith zero r_i of the Bessel function J_0 by

$$\Gamma_i = \left(\frac{r_i}{\theta_M}\right)^2.$$

It is noteworthy that the lowest order coefficient Γ_0 is smaller than the others. For long distances, when Z satisfies:

$$Z \gg \frac{1}{\Gamma_1 - \Gamma_0}$$

Only the first term of the expansion (16) remains. The steady-state solution of (14) simplifies to

$$P(\theta,Z) = \eta_0 \exp(-\Gamma_0 Z)J_0(\sqrt{\Gamma_0}\,\theta). \tag{17}$$

The attenuation is

$$\Gamma_0 = \left(\frac{2.405}{\theta_M}\right)^2$$

or, according to (15), in decibels per kilometer

$$\gamma_0(\text{dB/km}) = \frac{2.51\times 10^4 D_0}{{\theta_M}^2}. \tag{18}$$

Thus the steady-state radiation pattern is

$$P_{eq}(\theta) = J_0\left(2.405\,\frac{\theta}{\theta_M}\right). \tag{19}$$

This represents the exact analytical solution of (9) when the coupling coefficient is constant. It will be compared in Section IV with the numerical result obtained for the same condition.

III. Numerical Method

The numerical integration of (5) involves the segmentation of the θ and z axes to form a rectangular lattice. At each point (θ_j,z_k) of the grid the derivatives are approximated by difference formulas. Thus a set of finite-difference equations with $P(\theta_j,z_k)$ replaces the differential equation with $P(\theta,z)$.

First of all, the discretization of (5) poses the problem of the conditions for convergence and stability of the numerical solutions. Let A be the exact solution of the analytical equation, D be the exact solution of the finite difference equations, and N be the obtained numerical solution. The convergence implies that, as the mesh of the lattice becomes smaller, the discretization error $A - D$ tends to zero. The stability implies that the numerical error $D - N$ is as small as possible.

Discretization schemes with their convergence and stability criteria are known for linear parabolic differential equations with constant coefficients [5]. However, there are few schemes when we have variable coefficients, and we need to extrapolate the elementary formulas. Hence we extend the Crank–Nicholson implicit method which is unconditionally stable in the simple case and assures an excellent convergence.

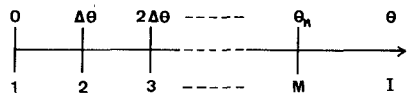

Fig. 1. Segmentation of the interval $[0,\theta_M]$.

The principle is as follows. The discretization of the right-hand side of (5) yields

$$\frac{\partial P}{\partial z} = f_D(\theta,P) + 0(\Delta\theta^P) \tag{20}$$

where $0(\Delta\theta^P)$ is the truncation error. Let P_0, $P_0 + \Delta P$ be the values of P for $z = z_0$ and for $z = z_0 + \Delta z$, respectively. At $z = z_0 + (\Delta z/2)$, we can write (20) in the form

$$\frac{\Delta P}{\Delta z} = \frac{f_D(\theta, P_0 + \Delta P) + f_D(\theta,P_0)}{2} + 0(\Delta\theta^P) + 0(\Delta z^2). \tag{21}$$

We now have to apply (21) to each point of the grid.

In order to clarify this discussion, we have only shown the finite-difference equations for the case $D(\theta) = D_0$. The determination of the equations for the general case is easily deduced but is algebraically more complex. Furthermore, we stress that the resolution method of the obtained equations is identical for any value of $D(\theta)$ in which we are interested.

As seen in Fig. 1, we divide the interval of interest $[0,\theta_M]$ into segments $[\theta_I,\theta_{I+1}]$ of identical lengths $\Delta\theta$ (this discretization step $\Delta\theta$ should not be confused with the angular separation $\delta\theta$ between modes). Thus

$$\theta_1 = 0 \qquad \theta_I = (I - 1)\,\Delta\theta. \tag{22}$$

To simplify the nomenclature, we define the point I as having the abscissa θ_I, and we denote

$$P(\theta_I,Z) = P^Z(I). \tag{23}$$

To obtain the finite-difference equation equivalent to (14), we must estimate: $(1/\theta)(\partial/\partial\theta)(\theta(\partial P/\partial\theta))$ at the point I. By repeated applications of the Taylor expansion, we readily find that

$$\begin{aligned}\frac{1}{\theta}\frac{\partial}{\partial\theta}\left(\theta\frac{\partial P}{\partial\theta}\right)\Bigg|_I &= \frac{(I - \tfrac{1}{2})P(I + 1) + 2(1 - I)P(I) + (I - \tfrac{3}{2})P(I - 1)}{(I - 1)\,\Delta\theta^2} \\ &\quad - \frac{\Delta\theta^2}{12}\left(\frac{\partial^4 P}{\partial\theta^4}\Big|_I + \frac{2}{\theta}\frac{\partial^3 P}{\partial\theta^3}\Big|_I\right) \\ &\quad - \frac{\Delta\theta^4}{360}\left(\frac{3}{\theta}\frac{\partial^5 P}{\partial\theta^5}\Big|_I + \frac{\partial^6 P}{\partial\theta^6}\Big|_I\right) \\ &\quad + 0\,(\Delta\theta^6).\end{aligned} \tag{24}$$

In most previous schemes, for simplification, the terms in $\Delta\theta^2$ and $\Delta\theta^4$ have been neglected. In our calculations, changes of $P(\theta,Z)$ as a function of θ can be extremely fast. For instance, this takes place if we select at $Z = 0$ a narrow angular power distribution. This implies large values of third and fourth derivatures, and in order to feature convergence would require very small $\Delta\theta$. On the other hand, small values of $\Delta\theta$ would lead to significant numbers of points M, to long computer times, or to instability. We circumvent this difficulty by retaining the term in $\Delta\theta^2$.

The coefficient of $\Delta\theta^2/12$ in (24) can be expressed as

$$\frac{\partial^4 P}{\partial\theta^4} + \frac{2}{\theta}\frac{\partial^3 P}{\partial\theta^3} = \frac{1}{\theta}\frac{\partial}{\partial\theta}\left(\frac{\partial^2 P}{\partial\theta^2} + \theta\frac{\partial^3 P}{\partial\theta^3}\right).$$

Using (14), we obtain

$$\frac{\partial^4 P}{\partial\theta^4} + \frac{2}{\theta}\frac{\partial^3 P}{\partial\theta^3} = \frac{\partial}{\partial Z}\left[\frac{1}{\theta}\frac{\partial}{\partial\theta}\left(\theta\frac{\partial P}{\partial\theta}\right)\right] + \frac{1}{\theta}\frac{\partial}{\partial\theta}\left(\frac{1}{\theta}\frac{\partial P}{\partial\theta}\right). \tag{25}$$

By substituting (25) into (24) and replacing the derivatives by difference formulas, we find

$$\begin{aligned}&\frac{1}{\theta}\frac{\partial}{\partial\theta}\left(\theta\frac{\partial P}{\partial\theta}\right)\Bigg|_I \\ &= P(I + 1)\left(\frac{12(I - \tfrac{1}{2})^2 - 1}{12(I - 1)(I - \tfrac{1}{2})\,\Delta\theta^2}\right) \\ &\quad - P(I)\left(\frac{12(I - \tfrac{1}{2})(I - \tfrac{3}{2}) - 1}{6(I - \tfrac{1}{2})(I - \tfrac{3}{2})\,\Delta\theta^2}\right) \\ &\quad + P(I - 1)\left(\frac{12(I - \tfrac{3}{2})^2 - 1}{12(I - 1)(I - \tfrac{1}{2})\,\Delta\theta^2}\right) \\ &\quad - \frac{1}{12(I - 1)}\frac{\partial}{\partial Z} \\ &\quad \cdot [(I - \tfrac{1}{2})P(I + 1) - 2(I - 1)P(I) + (I - \tfrac{3}{2})P(I - 1)] \\ &\quad + 0\,(\Delta\theta^4).\end{aligned} \tag{26}$$

Equation (14) at point I then becomes

$$\begin{aligned}&\frac{\partial}{\partial Z}[(I - \tfrac{1}{2})P(I + 1) + 10(I - 1)P(I) + (I - \tfrac{3}{2})P(I - 1)] \\ &\quad = \frac{12(I - \tfrac{1}{2})^2 - 1}{(I - \tfrac{1}{2})\,\Delta\theta^2}P(I + 1) \\ &\quad\quad + 2(1 - I)\left(\frac{12(I - \tfrac{1}{2})(I - \tfrac{3}{2}) - 1}{(I - \tfrac{1}{2})(I - \tfrac{3}{2})\,\Delta\theta^2}\right)P(I) \\ &\quad\quad + \frac{12(I - \tfrac{3}{2})^2 - 1}{(I - \tfrac{3}{2})\,\Delta\theta^2}P(I - 1) + 0\,(\Delta\theta^4).\end{aligned} \tag{27}$$

Let ΔZ be the discretization step of the Z axis. Referring back to the Crank–Nicholson scheme in (20) and (21), we obtain the set of equations

$$A(I)P^{Z+\Delta Z}(I - 1) + B(I)P^{Z+\Delta Z}(I) + C(I)P^{Z+\Delta Z}(I + 1) = K_0(I) \tag{28}$$

with

$$K_0(I) = D(I)P^Z(I - 1) + E(I)P^Z(I) + F(I)P^Z(I + 1). \tag{29}$$

The detailed calculation of coefficients A, B, C, D, E, F is described in the Appendix; it is shown that they only depend on I and on the ratio $\Delta\theta^2/\Delta Z$.

We avoid the problem of division by zero at $\theta = 0$ by using

$$\lim_{\theta \to 0} \frac{1}{\theta} \frac{\partial}{\partial \theta} \left(\theta \frac{\partial P}{\partial \theta} \right) = 2 \frac{\partial^2 P}{\partial \theta^2} \bigg|_{\theta = 0}.$$

We remark that

$$A(1) = D(1) = C(M-1) = F(M-1) = 0.$$

As has been previously observed with other generalized schemes [5 p. 193], the complete discretization error is of the order $\Delta\theta^4$ and ΔZ^2. This implies that a given accuracy is achieved with greater values of $\Delta\theta$ and ΔZ (i.e., less calculation) than required by the simpler formulas. It should be noted that the form of equations (28) and (29) is unaffected by the expansion to order 4 in $\Delta\theta$. However, a further reduction of the truncation error to ΔZ^3 or ΔZ^4 would lead to the introduction of unknowns $P^{Z+\Delta Z}(I+2)$ and $P^{Z+\Delta Z}(I-2)$, and to tremendous calculations for solving (28).

Equation (28) assumes that all values of $P(I)$ at length Z are known and gives values for P at length $Z + \Delta Z$. Hence with any initial state of power distribution, the power distribution at length $k\Delta Z$ can be calculated by solving the system (28) k times.

In order to solve (28), a first method consists of inverting the associated tridiagonal matrix of order $M-1$. This technique requires a long computer time and gives rise to roundoff errors. Therefore we prefer to use a very simple and efficient algorithm based on back substitution [5 p. 199].

It is shown that (28) can be written as

$$P^{Z+\Delta Z}(I) = S(I)[K_1(I) - C(I)P^{Z+\Delta Z}(I+1)]. \quad (30)$$

The recursion relationships for $S(I)$ and $K_1(I)$ are

$$S(I) = \frac{1}{B(I) - A(I)C(I-1)S(I-1)}$$

$$K_1(I) = K_0(I) - A(I)K_1(I-1)S(I-1) \quad (31)$$

with

$$S(1) = \frac{1}{B(1)}$$

$$K_1(1) = K_0(1). \quad (32)$$

The computation procedure is as follows. Once we have $S(I)$, $K_1(I)$ at mesh points 1 to $M-1$ from (31) and (32), we use (30) to find $P^{Z+\Delta Z}(M-1)$

$$P^{Z+\Delta Z}(M-1) = S(M-1)K_1(M-1)$$

and we work backward to find $P^{Z+\Delta Z}(M-2), \cdots P^{Z+\Delta Z}(1)$. Hence, knowing $P(\theta, Z+\Delta Z)$, we can obtain the total power $\mathcal{P}(Z+\Delta Z)$ by approximating (11) by the Simpson rule.

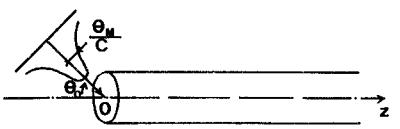

Fig. 2. Definition of the input beam parameters (angles are measured inside the fiber).

IV. Results

As an example, the computation reported herein uses

$$\theta_M = 0.130 \text{ rad.} \quad (33)$$

From (3) the relevant numerical aperture with a core index of 1.46 is 0.190, which is a reasonable value for Corning fibers [3], [4], [6]. However, the selected value of θ_M does not restrict the generality of our results. According to (9) and (37), they can be extended to the value

$$\theta_M = 0.130X$$

by simply multiplying the z scale by X^2 and the scale of the attenuation γ by $1/X^2$.

Although the method described allows for arbitrary launching conditions, results are presented for input distributions of the form

$$P(\theta,0) = \exp\left[- \left(\frac{\theta - \theta_0}{\theta_M} \right)^2 C^2 \right] \quad (34)$$

with

$$0 \le \theta_0 \le \theta_M$$

$$0 \le C \le 10.$$

As shown in Fig. 2, this corresponds to a Gaussian beam with an incidence θ_0 and a width θ_M/C. (Angles are defined inside the fiber core.) It is noteworthy that at the lower limit $C = 0$, the guided modes are equally excited, as in the case of the light emitting diode (LED).

With such initial conditions, it has been observed in all the tested cases that the best compromise (computer time accuracy) is achieved when

$$M = 82$$

$$\frac{\Delta Z}{\Delta \theta^2} = 4.6.$$

In an attempt to measure the computation stability at every Z step, we calculate separately both sides of (12). The relative difference obtained is always less than 6×10^{-3}.

Uniform Coupling Coefficient

As an example, the parameter characterizing the mode coupling is

$$D(\theta) = D_0 = 2.92 \times 10^{-6} \text{ (rad)}^2/\text{m}. \quad (35)$$

This yields from (18) and (33) a very simple value of the steady-state attenuation:

$$\gamma_0 = 4.34 \text{ dB/km} = 1 \text{ km}^{-1}. \quad (36)$$

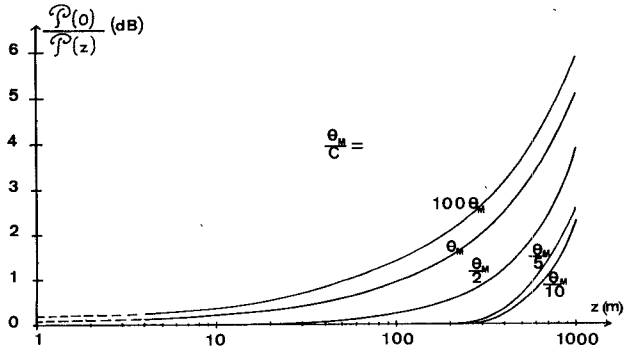

Fig. 3. Total optical loss versus length for various Gaussian input beams: $\exp(-\theta^2C^2/\theta_M{}^2)$.

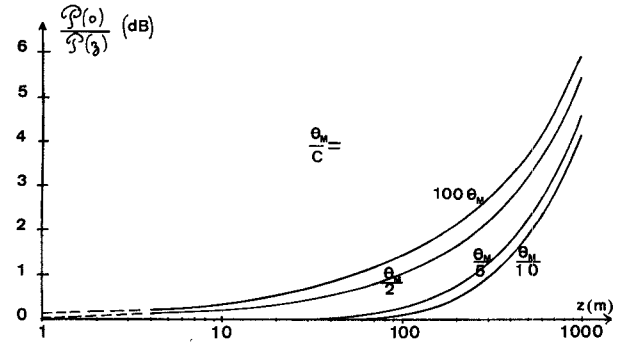

Fig. 4. Total optical loss versus length for various Gaussian input beams: $\exp(-(\theta/\theta_M - \frac{1}{2})^2C^2)$.

As previously mentioned for θ_M, complete freedom is available in the choice of D_0. Straightforward extension to

$$D(\theta) = 2.92 \times 10^{-6}Y$$

may be achieved by multiplying the z scale by $1/Y$ and the attenuation scale by Y.

The relevant results are fairly numerous. We want to present the powerfulness of the method and to point out the available specific parameters. For two values of the incidence angle θ_0: 0, $\theta_M/2$ and various widths θ_M/C of the input beam, we show the variations versus length:

—of the total optical loss on Figs. 3 and 4 $[\mathcal{P}(0)/\mathcal{P}(z)]$;

—of the attenuation per unit length in Figs. 5 and 6

$$\alpha = \frac{4.34}{\mathcal{P}(z)}\frac{d\mathcal{P}(z)}{dz} \text{ (dB/km)} \tag{37}$$

—of the normalized radiation pattern in Figs. 7 and 8.

We can verify that numerical and analytical results are in very good agreement. Independently of the input beam, the power reaches the steady-state distribution given from (17) by

$$P(\theta,z) = \exp(-\gamma_0 z)J_0\left(2.405\frac{\theta}{\theta_M}\right).$$

The predicted steady-state radiation pattern is actually observed on the curves $z = \infty$ in Figs. 5 and 6 and the attenuation γ_0 is obtained on asymptotical lines in Figs. 7 and 8. Moreover, to give a measure of accuracy of the

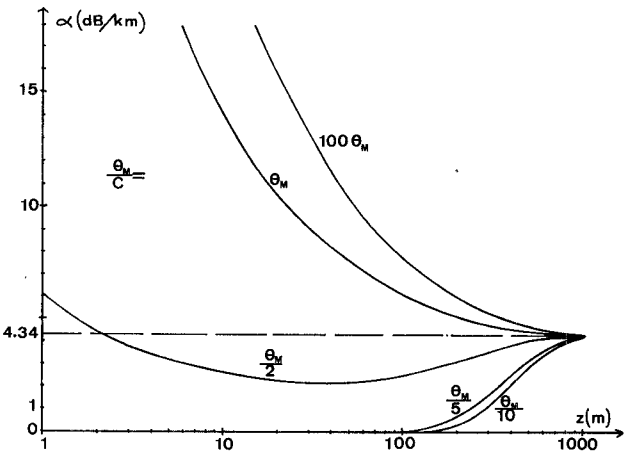

Fig. 5. Attenuation versus length for various Gaussian input beams: $\exp(-\theta^2C^2/\theta_M{}^2)$.

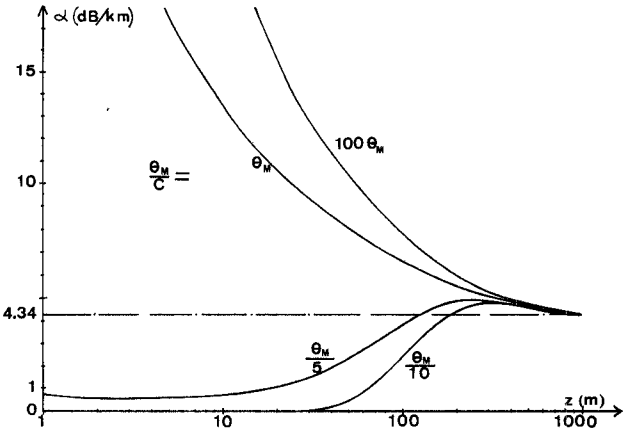

Fig. 6. Attenuation versus length for various Gaussian input beams: $\exp(-(\theta/\theta_M - \frac{1}{2})^2C^2)$.

method for all θ and z, it is convenient to select at $z = 0$ a basic distribution

$$P(\theta,0) = J_0(\sqrt{\Gamma_i}\theta)$$

and to observe throughout the length of the fiber the deviation between the analytical solution deduced from (15) and (16):

$$P_A(\theta,z) = \exp(-\Gamma_i D_0 z)J_0(\sqrt{\Gamma_i}\theta)$$

and the numerical solution $P_N(\theta,z)$. It should be noted that the input distribution can be negative for $i \geq 1$ so that the relevant solutions have no physical significance. For $i = 0$ and all values of θ and z, we obtain

$$\left|\frac{P_A(\theta,z) - P_N(\theta,z)}{P_A(\theta,z)}\right| < 5 \times 10^{-5}.$$

In the other cases ($i \geq 1$), if the total loss is less than 20 dB (which yields z(km) $\leq (1.6 \times 10^3/\Gamma_i)$), we obtain

$$\left|\frac{P_A(\theta,z) - P_N(\theta,z)}{P_A(\theta,z)}\right| < 2 \times 10^{-3}.$$

These results are quite satisfactory and show the efficiency of the method; however, a further improvement can be achieved by reducing $\Delta\theta$ and Δz.

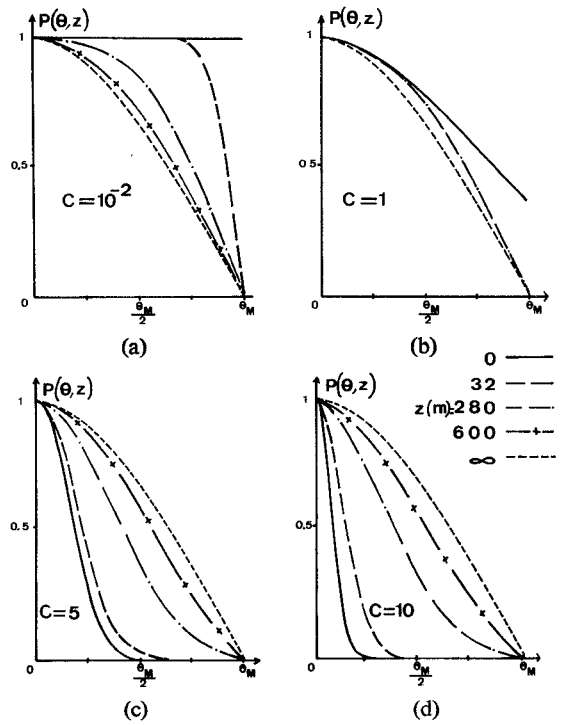

Fig. 7. Radiation pattern at different lengths for various Gaussian input beams: $\exp(-\theta^2C^2/\theta_M^2)$. (a) $C = 10^{-2}$. (b) $C = 1$. (c) $C = 5$. (d) $C = 10$.

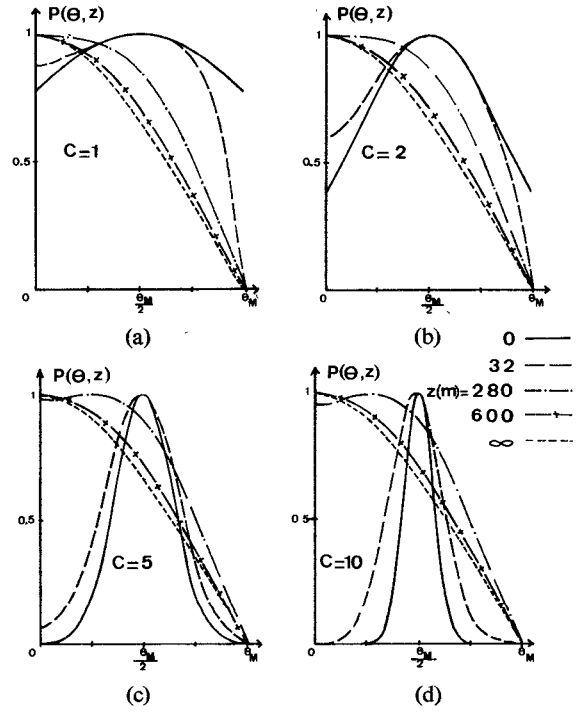

Fig. 8. Radiation patterns at different lengths for various Gaussian input beams: $\exp(-(\theta/\theta_M - \frac{1}{2})^2C^2)$. (a) $C = 1$. (b) $C = 2$. (c) $C = 5$. (d) $C = 10$.

The study of the radiation pattern and the attenuation shows that the distance z_e that is required to reach the steady state is virtually independent of the parameters of the input Gaussian beam. We find

$$z_e \simeq 1 \text{ km}.$$

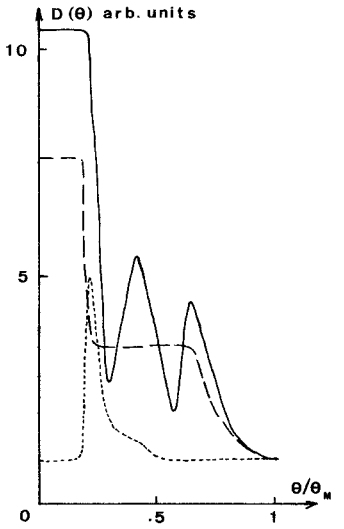

Fig. 9. Mode coupling coefficient measured for three different buffered Corning fibers.

On the other hand, at this length the total optical loss is strongly dependent on the initial conditions. For instance, the extreme losses obtained at $z = z_e$ are

$$2.4 \text{ dB with } \theta_0 = 0 \ , C = 10$$

$$13.6 \text{ dB with } \theta_0 = \theta_M, C = 10.$$

The more interesting case (i.e., the smaller loss) occurs when the input beam is very narrow and centered on the z axis.

These results indicate that it is impossible to characterize a given fiber by its overall loss without specifying the input launching distribution.

Variable Coupling Coefficient

Most of our experimental measurements on buffered Corning fibers [3] show that the coupling coefficient as a function of θ initially decreases and remains virtually constant in the vicinity of θ_M (Fig. 9). In order to take the various magnitudes and rates of decrease into account, we consider two types of coupling coefficients:

$$\textit{Type 1)}: D_1(\theta) = D_0\left(1 + h\cos\left(\frac{\pi}{2}\frac{\theta}{\phi}\right)\right), \qquad 0 \le \theta \le \phi \le \theta_M$$

$$= D_0, \qquad \phi < \theta \le \theta_M. \tag{38}$$

$$\textit{Type 2)}: D_2(\theta) = D_0\left(1 + h\cos^2\left(\frac{\pi}{2}\frac{\theta}{\phi}\right)\right), \qquad 0 \le \theta \le \phi \le \theta_M$$

$$= D_0, \qquad \phi < \theta \le \theta_M \tag{39}$$

with

$$h = 1,2,\cdots,10$$

$$\phi = \frac{\theta_M}{4}, \frac{\theta_M}{2}, \frac{3\theta_M}{4}, \theta_M.$$

The physical mean of parameters h and ϕ is sketched in Fig. 10. As already noted, we can find and plot the length

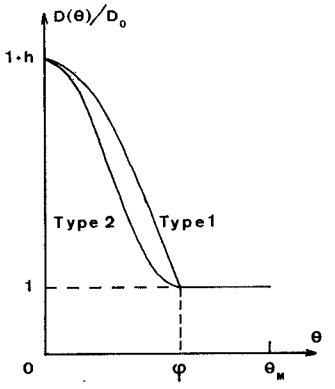

Fig. 10. Theoretical mode coupling coefficients for buffered Corning fibers.

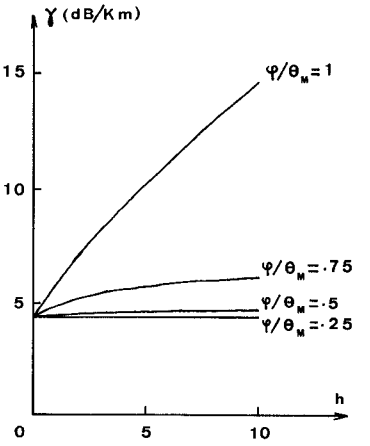

Fig. 11. Steady-state attenuation due to mode coupling versus h for type 1.

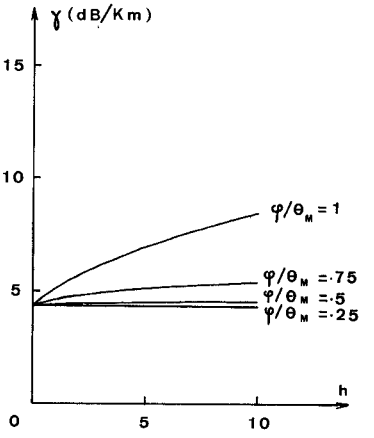

Fig. 12. Steady-state attenuation due to mode coupling versus h for type 2.

dependence of the principal unknowns: total loss, attenuation, and radiation pattern. But to clarify the following discussion, we are only concerned with two basic quantities.

1) The steady-state attenuation per unit length is defined by

$$\gamma = \lim_{z\to\infty} \frac{4.34}{\mathscr{P}(z)} \frac{d\mathscr{P}(z)}{dz}. \tag{40}$$

The numerical value of D_0 is given in (35) and yields for $h = 0$: $\gamma = 4.34$ dB/km (bearing in mind that the multiplication of D_0 by the factor Y implies the multiplication of the z scale by $1/Y$ and the γ scale by Y).

2) The effective width of the radiation pattern $\theta_{\text{eff}}(z)$ is defined as the semiangle of the cone which contains 90 percent of the total power $\mathscr{P}(z)$. From (11) $\theta_{\text{eff}}(z)$ is the solution of the equation

$$\frac{\int_0^{\theta_{\text{eff}}} \theta P(\theta,z)\, d\theta}{\int_0^{\theta_M} \theta P(\theta,z)\, d\theta} = 0.9. \tag{41}$$

The variations of γ with h for the different values of ϕ are shown in Fig. 11 for the first type of coupling coefficient and in Fig. 12 for the second. In both cases we observe that the steady-state attenuation does not change greatly with increasing h, as long as ϕ is below $\theta_M/2$ (from (33) $\phi <$ 0.065 rad). If we assume that mode coupling is mainly due to random microbends of the fiber axis induced in the buffering process, this means, referring to the power spectrum of the curvature function [3], [7], that mechanical correlation length must be kept above 3 mm. When imperfections with smaller mechanical wavelength are introduced, the attenuation becomes very sensitive to the magnitude h, but for high values of h tends to saturation. Moreover, the comparison of Figs. 11 and 12 indicates that for a given value of ϕ, the increase of γ with h is faster in the first case than in the second.

A consequence of these results is that, as far as possible, we have to prevent the formation of defects with short wavelength because, even if their magnitude is small (for instance $h = 1$), they dramatically influence the attenuation. The long wavelength defects (i.e., > 3 mm) are much less restricting, since the relative increase of attenuation is less than 10 percent. Although the presence of the former cannot be avoided in practice, we can limit their effect, upon the differences between cases 1 and 2, by modifying the shape of the power spectrum and consequently of $D(\theta)$.

Then by retaining the coupling coefficient of type 2, we show in Fig. 13(a) the length dependence of the effective width of the radiation pattern for $h = 5$ and for several values of ϕ. In order to observe important changes, we select a rather narrow launching beam with $\theta_{\text{eff}}(0) = 0.3\ \theta_M$. Two things which are quite intuitive are of interest: a large value of ϕ results in a fast evolution of $\theta_{\text{eff}}(z)$ and the increase of the steady-state value of θ_{eff} with ϕ is perceptible only for ϕ greater than $\theta_M/2$.

In order to measure the rate of evolution, it is convenient to introduce the parameter γ_∞ [6] which is virtually independent of the input conditions. It is related to the distance z_e required to reach the steady state by

$$\gamma_\infty \simeq \frac{2}{z_e}. \tag{42}$$

The numerical values of γ_∞ compared with the corresponding value of γ as functions of ϕ are as follows:

$$\phi = 0, \frac{\theta_M}{4} \qquad \frac{\gamma_\infty}{\gamma} = 3$$

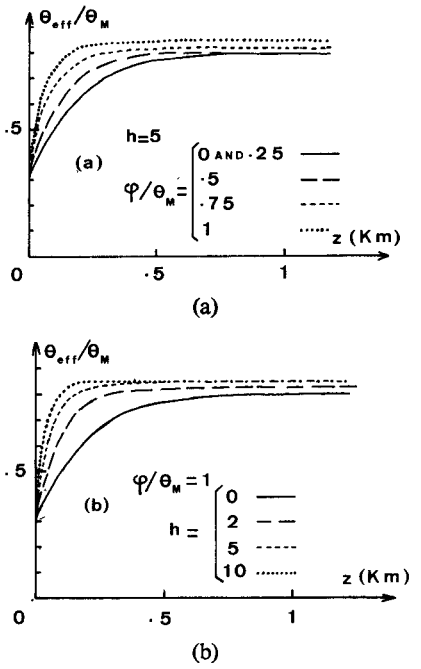

Fig. 13. Effective width of the far-field radiation pattern versus length for different values h and ϕ (type 2). (a) $h = 5$. (b) $\phi/\theta_M = 1$.

$$\phi = \frac{\theta_M}{2} \qquad \frac{\gamma_\infty}{\gamma} = 4.27$$

$$\phi = \frac{3\theta_M}{4} \qquad \frac{\gamma_\infty}{\gamma} = 5.04$$

$$\phi = \theta_M \qquad \frac{\gamma_\infty}{\gamma} = 5.2.$$

In this way it is worth noting that our results are in a good agreement with an analytical relationship obtained with the main assumption of a constant coupling coefficient [6]

$$\frac{\theta_{\text{eff}}^2(z)}{\theta_{\text{eff}}^2(\infty)} = \frac{\theta_{\text{eff}}^2(0) + \theta_{\text{eff}}^2(\infty) th \gamma_\infty z}{\theta_{\text{eff}}^2(\infty) + \theta_{\text{eff}}^2(0) th \gamma_\infty z} \tag{43}$$

where $\theta_{\text{eff}}(\infty)$ is the steady-state value of θ_{eff}. Likewise Fig. 13(b) shows the length dependance of effective width for $\phi = \theta_M$ and for several values of h. The rates at which the steady states are reached as functions of h are as follows:

$$h = 0 \qquad \frac{\gamma_\infty}{\gamma} = 3$$

$$h = 2 \qquad \frac{\gamma_\infty}{\gamma} = 4.23$$

$$h = 5 \qquad \frac{\gamma_\infty}{\gamma} = 5.2$$

$$h = 10 \qquad \frac{\gamma_\infty}{\gamma} = 7.03.$$

We observe that γ_∞ and $\theta_{\text{eff}}(\infty)$ increase with h but also that $\theta_{\text{eff}}(\infty)$ tends to saturation.

V. Conclusion

Under the assumptions of mode coupling occurring between nearest neighbors and a differential attenuation being zero from 0 to θ_M and infinite beyond θ_M, we have developed a numerical method of solution of the power-flow equation in optical fibers.

Although we were obliged to take the high magnitude of the derivatives into account, the method is simple and easy to program. Moreover, its small memory requirements allow the use of small digital computers.

Solutions for the basic parameters (power distribution, attenuation, and far-field radiation pattern) are sought throughout the whole length of the fiber under arbitrary coupling coefficients and launching conditions. By introducing a correction factor on the power distribution, the method could be fruitfully applied to find the quantitative influence of a fiber joint or a local defect.

However, the presented results dealt mainly with buffered Corning fibers. It has been shown that with a constant coupling coefficient the numerical and analytical solutions are in complete agreement and that the distortions in fiber axis with correlation lengths less than 3 mm cause significant excess losses. We feel that these results are very important in the design of the buffering of Corning fibers.

Two further extensions of this work seem desirable: the determination of the optimal coupling coefficient shape and the solution of the time-dependent equation.

Appendix

By applying the Crank–Nicholson scheme described in (20) and (21), (27) can be written

$$\begin{aligned}\frac{\Delta\theta^2}{\Delta Z}&\left[(I-\tfrac{1}{2})(P^{Z+\Delta Z}(I+1)-P^Z(I+1))\right.\\&+10(I-1)(P^{Z+\Delta Z}(I)-P^Z(I))\\&\left.+(I-\tfrac{3}{2})(P^{Z+\Delta Z}(I-1)-P^Z(I-1))\right]\\&=\frac{(12(I-\tfrac{1}{2})^2-1)}{2I-1}[P^{Z+\Delta Z}(I+1)+P^Z(I+1)]\\&+\frac{(1-I)(12(I-\tfrac{1}{2})(I-\tfrac{3}{2})-1)}{(I-\tfrac{1}{2})(I-\tfrac{3}{2})}\\&\cdot[P^{Z+\Delta Z}(I)+P^Z(I)]\\&+\frac{12(I-\tfrac{3}{2})^2-1}{2I-3}[P^{Z+\Delta Z}(I-1)+P^Z(I-1)].\end{aligned} \tag{A1}$$

Let

$$\lambda = 2\frac{\Delta\theta^2}{\Delta Z}. \tag{A2}$$

Equation (A1) can be rewritten in a standard form as

$$\begin{aligned}A(I)P^{Z+\Delta Z}(I-1)&+B(I)P^{Z+\Delta Z}(I)+C(I)P^{Z+\Delta Z}(I+1)\\&=D(I)P^Z(I-1)+E(I)P^Z(I)+F(I)P^Z(I+1)\end{aligned} \tag{A3}$$

with

$$C(I) = \lambda\left(I - \frac{1}{2}\right) + \frac{1 - 12(I - \frac{1}{2})^2}{(I - \frac{1}{2})}$$

$$B(I) = 10\lambda(I - 1) + \frac{2(I - 1)[12(I - \frac{1}{2})(I - \frac{3}{2}) - 1]}{(I - \frac{1}{2})(I - \frac{3}{2})} \tag{A4}$$

and

$$A(I) = C(I - 1)$$

$$F(I) = -C(I) + \lambda(2I - 1)$$

$$E(I) = -B(I) + 20\lambda(I - 1)$$

$$D(I) = F(I - 1).$$

The first boundary condition (10) is satisfied with

$$C(M - 1) = F(M - 1) = 0. \tag{A5}$$

This set of equations is valid for $I = 2, \cdots M - 1$. For $I = 1$, in order to include the second boundary condition, we use expansions. We get

$$A(1) = D(1) = 0$$

$$B(1) = \lambda + 4$$

$$C(1) = -4$$

$$E(1) = \lambda - 4$$

$$F(1) = 4. \tag{A6}$$

References

[1] D. Gloge, "Optical power flow in multimode fibers," *B.S.T.J.*, vol. 51, pp. 1767–1783, Oct. 1972.

[2] ——, "Impulse response of clad optical multimode fibers," *B.S.T.J.*, vol. 52, pp. 801–816, July/Aug. 1973.

[3] L. Jeunhomme and J. P. Pocholle, "Angular dependence of the mode coupling coefficient in a multimode optical fiber," *Electron. Lett.*, vol. 11, pp. 425–426, Sept. 1975.

[4] D. B. Keck, "Spatial and temporal power transfer measurements on a low-loss optical waveguide," *Appl. Opt.*, vol. 13, pp. 1882–1888, Aug. 1974.

[5] R. D. Richtmyer and K. W. Morton, *Difference Methods for Initial Value Problems*, 2nd ed. New York: Interscience, 1967.

[6] L. Jeunhomme, M. Fraise, and J. P. Pocholle, "Propagation model for long step index optical fibers," *Appl. Opt.*, Dec. 1976.

Modes and Cutoff Frequencies of Crossed Rectangular Waveguides

QUANG C. THAM, MEMBER, IEEE

Abstract—**One complete solution is presented for determining the electromagnetic field of a generalized crossed rectangular waveguide. The method adopted is that of partial regions. Cutoff frequencies of symmetrical crossed waveguides are presented as an example. The results, even for low-order approximations, correspond well with the only experimental results available in the literature.**

I. Introduction

PRACTICAL waveguides usually have rectangular or circular cross sections whose cutoff frequencies and field equations have been known for years through the method of separation of variables. Other cross-sectional shapes are possible, but in general few of these have been investigated. Recently, crossed rectangular waveguide shapes have been of interest due to the fact that they may offer some advantages in terms of circular polarization and wider bandwidth or both [1]. Moreover, it has been shown experimentally that a dichroic panel of symmetrical crossed rectangular slots offers some favorable results as far as bandwidth and transmission at oblique angles of incidence are concerned [2].

The knowledge of crossed rectangular waveguides is, to the best knowledge of the author, limited to the paper by Stalzer *et al.* [1] who use a computer program developed by Konrad and Silvester [3] to calculate cutoff frequencies and field patterns. They also performed experimental work on the measurement of individual modes. Mathematical expressions for fields inside a crossed rectangular waveguide have not been reported.

Mathematical expressions for the fields within the guide are important. For example, if one is interested in modal matching techniques [4], [5] to give predictions for transmission of electromagnetic waves through a thin conducting screen periodically perforated with crossed rectangular slots, one has to know these relations.

The intent of this report is to find cutoff frequencies and expressions for the fields within the waveguide. Cutoff frequencies of symmetrical crossed waveguide shapes are presented in the form of graphs. The results, even for a 3×3 approximation, correspond well with the experimental results reported [1].

The generalized crossed rectangular waveguide studied in

Manuscript received July 19, 1976; revised October 14, 1976. This work was supported by the Goddard Space Flight Center, Greenbelt, MD, under Contract NAS5-23000.

The author is with the Antenna Engineering Section, Bendix Field Engineering Corporation, Columbia, MD 21045.